

Article

Regenerable Subnanometer Pd Clusters on Zirconia for Highly Selective Hydrogenation of Biomass-Derived Succinic Acid in Water

Chi Zhang, Wenrong Cao, Hongye Cheng, Lifang Chen * and Zhiwen Qi

State Key Laboratory of Chemical Engineering, School of Chemical Engineering, East China University of Science and Technology, Shanghai 200237, China; colin.zhang.ecust@gmail.com (C.Z.); wrcao_ecust@163.com (W.C.); hycheng@ecust.edu.cn (H.C.); zwqi@ecust.edu.cn (Z.Q.)

* Correspondence: lchen@ecust.edu.cn; Tel.: +86-21-6425-0935

Academic Editor: Leonarda F. Liotta

Received: 8 June 2016; Accepted: 4 July 2016; Published: 7 July 2016

Abstract: The size of metal particles is an important factor to determine the performance of the supported metal catalysts. In this work, we report subnanometer Pd clusters supported on zirconia by the microwave-assisted hydrothermal method. The presence of subnanometer Pd clusters on the zirconia surface was confirmed by two-dimensional Gaussian-function fits of the aberration-corrected high-angle annular dark-field images. These subnanometer Pd catalysts exhibit high catalytic performance for the hydrogenation of biomass-derived succinic acid to γ -butyrolactone in water and avoid the formation of overhydrogenated products, such as 1,4-butanediol and tetrahydrofuran. The catalyst with an ultra-low Pd loading of 0.2 wt. % demonstrated high selectivity (95%) for γ -butyrolactone using water as a solvent at 473 K and 10 MPa. Moreover, it can be reused at least six times without the loss of catalytic activity, illustrating high performance of the small Pd clusters.

Keywords: succinic acid hydrogenation; aqueous phase; subnanometer; Pd catalyst

1. Introduction

Supported Pd catalysts are widely used in many important commercial chemical processes such as oil refining and exhaust gas treatment [1–4]. Subnanometer clusters with a few metal atoms in each cluster and a particle size of less than 2 nm as a catalytic species on solid support are found to play a major role in oxidation or hydrogenation reactions [5,6]. However, the stability and recyclability remain a challenge because the isolated clusters or single atoms are mobile and readily sintered under high reaction temperatures [7]. To the best of our knowledge, there are only a few contributions regarding the atomically dispersed Pd catalysts that are active and stable at high temperatures [8,9], while those of Au and Pt catalysts have been widely reported [10–13]. Atomically dispersed Pd on graphene shows excellent durability against deactivation during 100 h of reaction time [8]. Peterson et al. [9] prepared Pd species on La-doped γ -alumina supports that can be easily regenerated at 973 K through oxidation using air. Moreover, the addition of atomically dispersed La^{3+} ions into the alumina support plays a key role in helping to stabilize and disperse isolated Pd atoms on the alumina surface.

As a promising alternative resource, biomass-derived molecules are widely available and renewable and can be converted into chemicals, medicines and fuels for vehicles. Succinic acid (SUC) as one of the most interesting biomass-derived platform chemicals can be generated via bioprocessing [14–16]. The hydrogenation of SUC to produce valuable C4 compounds, including γ -butyrolactone (GBL), tetrahydrofuran (THF) and 1,4-butanediol (BDO), has attracted significant interest for the broad market of the downstream industries [15]. In particular, GBL is a valuable

intermediate for producing C4 chemicals, polymers, solvents, pesticides and so forth [17]. Therefore, it is valuable to develop green and efficient processes for converting biomass-derived SUC into GBL.

Several supported catalysts have been reported to improve the efficiency of converting biomass-derived SUC into GBL [18,19]. Palladium-based catalysts are considered one of the most efficient catalysts because of their high catalytic activity and selectivity [20–22]. In addition, some factors such as support properties [23], the addition of a second metal [24] and the choice of solvent [25,26] were considered to improve the catalytic performance of Pd catalysts. However, these reported catalytic processes were either performed in the presence of organic solvents (1,4-dioxane or ethanol) or involved high Pd loadings (2.0%–5.0%), resulting in low Pd atom utilization efficiency and conflict with stringent environmental concerns. Such disadvantages make it important to design and cultivate catalysts with low Pd loading in green solvents for the liquid-phase hydrogenation of SUC.

As the fermentation broth contains over 95.0 wt. % water in the process of bio-fermentation for SUC generation [15], water as a solvent in the selective hydrogenation reaction of SUC can alleviate the risk of handling organic solvents and the expensive separation of SUC, which provides an economical process for SUC transformation. However, for the reaction taking place in water, the catalytic performance is poor as compared to organic solvents. Therefore, it remains a challenge to manufacture highly efficient catalysts in water for the hydrogenation of SUC [24,27–30].

In this work, we prepared subnanometer Pd clusters supported on zirconia by a microwave hydrothermal method. The obtained subnanometer Pd clusters on zirconia were found to achieve high activity and stability for the SUC hydrogenation to GBL using water as a solvent. Furthermore, the catalyst is regenerable and can be cycled several times without loss of its catalytic activity.

2. Results and Discussion

2.1. Electron Microscopy

Aberration-corrected high-angle annular dark-field scanning transmission electron microscopy (AC-HAADF-STEM) can recognize the atomically dispersed noble metal on the support, providing direct information about the surface structure of the catalysts [9,31,32]. Here, it was employed to characterize the dispersion and identification of the Pd clusters in the materials. The typical AC-HAADF-STEM image of 0.2 Pd/ZrO₂ as well as the size distribution is shown in Figure 1a and additional representative images are present in Figure S1 in the Supplementary Materials (SM). In our previous works [33], the relationship between the cluster sizes and the numbers of Pd atoms in the clusters were determined by density functional theory calculation. Actually, the number of atoms is not directly relative to the horizontal projected area from the AC-HAADF-STEM images due to the difference in the layer stacking. From the reported EXAFS experiments on Pd clusters [34], the spherical Pd particles with a size less than 0.83 nm contain a maximum of 13 atoms. The major Pd species (>90%) represent subnanometer clusters based on statistical results over 400 Pd particles in 0.2 Pd/ZrO₂ catalyst with diameters <0.90 nm [13]. The bright spots (marked 1 and 2 in Figure 1b,c) correspond to Pd particles, while the gray areas are zirconia nanospheres with a surface area of 216 m²·g⁻¹ according to the Brunauer-Emmett-Teller (BET) method (Figure S2). In the selected and enlarged area (Figure 1b), the size of dispersed Pd species in the catalyst is about 0.45 nm. However, the varying background from the zirconia support limits this technology for locating the isolated Pd species in the catalyst.

The overlapped atom intensities are fitted using two-dimensional (2D) Gaussian functions by facile background subtraction so that the subnanometer Pd cluster can be recognized clearly in the AC-HAADF-STEM images (Figure 1c–e) [9]. It is known that the contrast of atoms in AC-HAADF-STEM is generated from the nucleus by electron scattering. The resulting distinct intensity is relative directly to the square of the metal atomic number. The enlarged area in the original AC-HAADF-STEM image (Figure 1c) was colorized according to the intensity after 2D Gaussian function fits. The brightest part was colored in red while blue corresponds to the darkest

part (Figure 1d). Then, the Pd particles can be easily identified in Figure 1e with the colorized intensity map. The histogram of intensity (Figure 1f) from Figure 1e shows a two-peak distribution of the two monodisperse species. The same intensity of the two peaks indicates the two dots (1 and 2) in Figure 1c only contain Pd species.

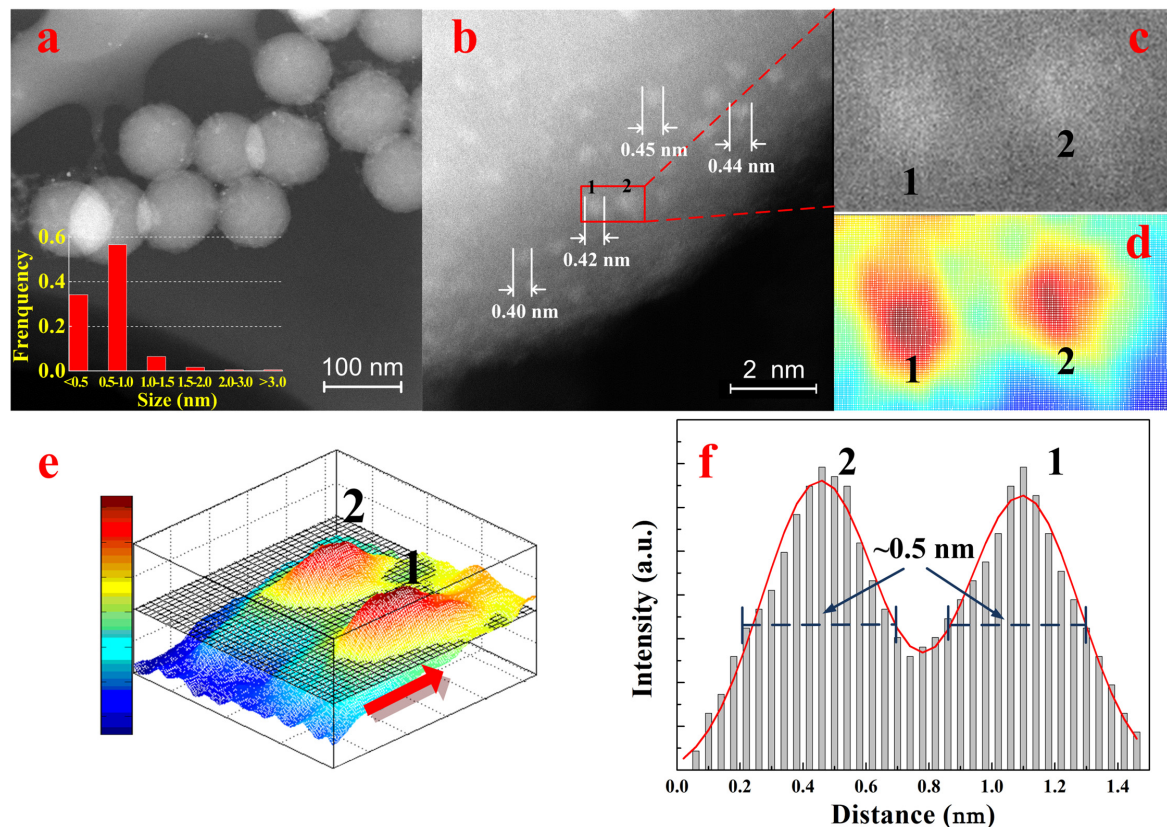


Figure 1. The typical Aberration-corrected high-angle annular dark-field scanning transmission electron microscopy (AC-HAADF-STEM) image and size distribution: (a) a selected and enlarged region from (a); (b) an enlarged area from (b); (c) a colorized intensity map from (c); (d) 2D Gaussian function fits to the intensity maps (e) and normalized intensity distributions received from the image (e) along arrow direction (f) of the 0.2 Pd/ZrO₂ catalyst. The size distribution (inset in (a)) was based on over 400 Pd clusters from the high-magnification images. The two Pd clusters in (b) were designated 1 and 2, respectively.

In this histogram, the diameter of the Pd particles is about 0.50 nm, which is larger than that of the direct identification from the origin images (Figure 1b) owing to the background subtraction through the image analysis. Efremenko et al. [35] have reported that Pd clusters contain two to four atoms with a diameter less than 0.50 nm. So the Pd cluster marked 1 in Figure 1b with a size of 0.50 nm may contain two to four atoms. Our previous work [33] has also found similar results depending on the layer stacking.

In addition, the density of Pd atoms, calculated from the counted Pd atoms divided by the total surface area of ZrO₂ in the AC-HAADF-STEM images, is about 0.048 Pd atoms·nm⁻² for 0.2 Pd/ZrO₂. It is very close to the actual Pd density (0.053 Pd atoms·nm⁻²), which is calculated from the number of supported Pd atoms in the catalyst over the total surface area of ZrO₂ obtained by the BET method. The little difference between these two densities confirms there is only one layer of Pd atoms on the ZrO₂ surface according to the radius of Pd. Thus, the observed Pd clusters are dispersed on the ZrO₂ surface or the near subsurface [31].

Figure 2a shows the X-ray diffraction (XRD) patterns of a series of Pd/ZrO₂ catalysts, all of which exhibit a tetragonal ZrO₂ (JCPDF No. 81-1549, Figure S3) structure with high crystallinity. Besides, the peak at 28° in the sample prepared by the conventional hydrothermal method (ZrO₂-hydrothermal) is the characteristic peak of the monoclinic phase (JCPDF No. 72-1669).

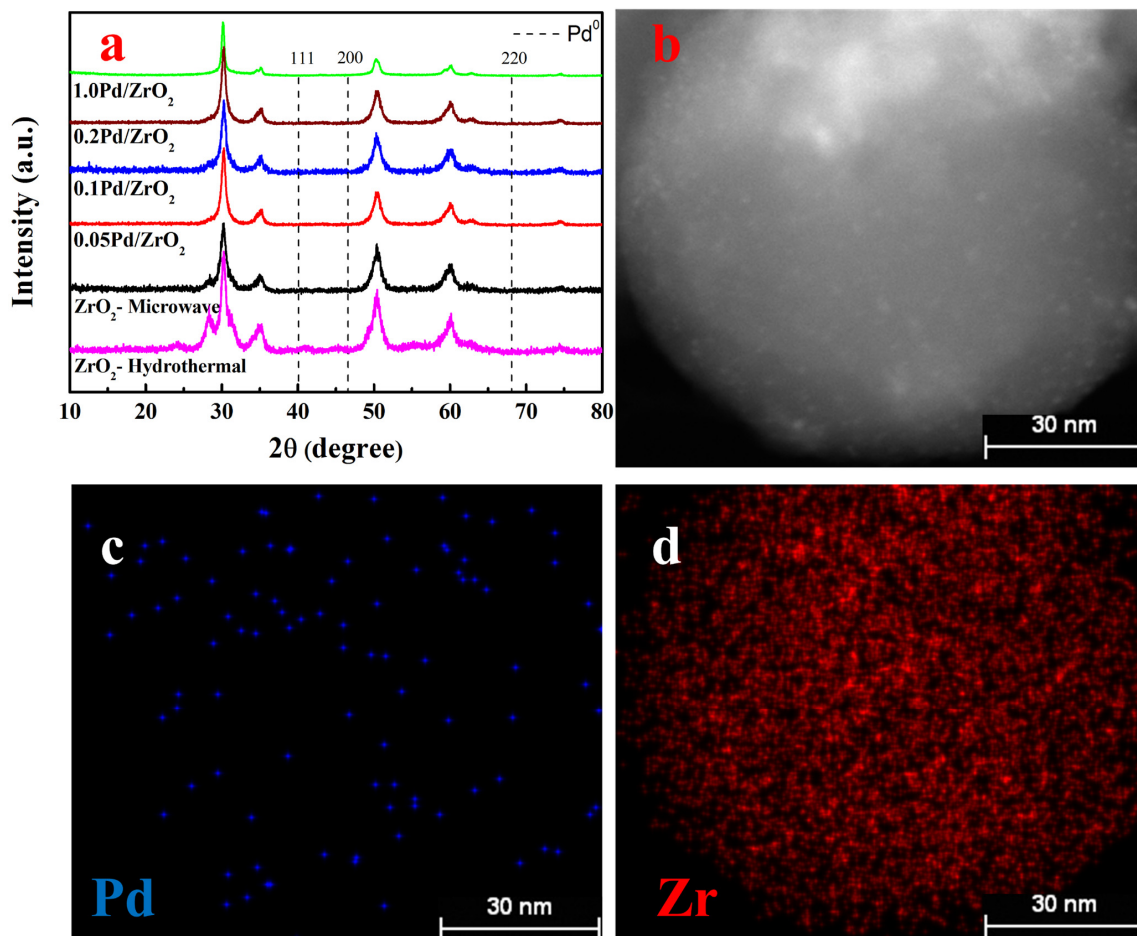


Figure 2. X-ray diffraction patterns of Pd/ZrO₂ (a); AC-HAADF-STEM image of 0.2 Pd/ZrO₂ catalyst (b); energy-dispersive X-ray element mapping images for Pd (c) and Zr (d).

Microwaves are electromagnetic waves containing electric and magnetic field components. Therefore, microwaves can provide fast heating, thus dramatically reducing reaction times and enhancing crystallized purity of the material produced [36,37]. Further, no obvious peaks ascribed to Pd at 41°, 55° and 68° were observed, which indicates that the Pd species are well dispersed on the support. This phenomenon is attributed to the microwave heating for the hydrothermal synthesis of the noble metal clusters [38]. Thus, it can be inferred that microwave heating leads to Pd species with a narrow size distribution and good dispersity on ZrO₂ nanospheres. Moreover, energy-dispersive X-ray mapping measurements were conducted (Figure 2c,d) to examine the elemental distribution of Pd species in the 0.2 Pd/ZrO₂ catalyst. The element mapping images indicate the bright dots in AC-HAADF images are Pd clusters (Figure 2b), which coincided well with the result of AC-HAADF images analysis.

2.2. Catalytic Activity of Pd/ZrO₂

The heterogeneous Pd-based catalysts are efficient in the hydrogenation of SUC to GBL using organic solvents, e.g., 1,4-dioxane and ethanol [39–41]. As the fermentation process for SUC generation

is performed in water [15], it would be more economical to perform the SUC hydrogenation reaction directly in aqueous media with a heterogeneous catalyst.

The zirconia-supported subnanometer Pd clusters were utilized for the selective hydrogenation of SUC to GBL in water. In the reaction, GBL is the main product while propionic acid (PA) and butanoic acid (BA) are produced as byproducts. The catalytic results are shown in Table 1 and Figure S4. The support exhibits no catalytic activity for SUC hydrogenation (Table 1, entry 1). However, SUC conversion reaches 34% with GBL selectivity as high as 99% for 0.1 Pd/ZrO₂. In contrast, SUC conversion increases from 63% to 99% and GBL selectivity drops from 95% to 85% with increased Pd loadings (0.2 wt. % to 1.0 wt. %). The byproducts are acids with 2.7 mol. % and 9.6 mol. % of BA, 1.6 mol. % and 4.5 mol. % of PA over 0.2 Pd/ZrO₂ and 1.0 Pd/ZrO₂, respectively.

Table 1. Catalytic activity of Pd/ZrO₂ and reported Pd catalysts for the hydrogenation of succinic acid.

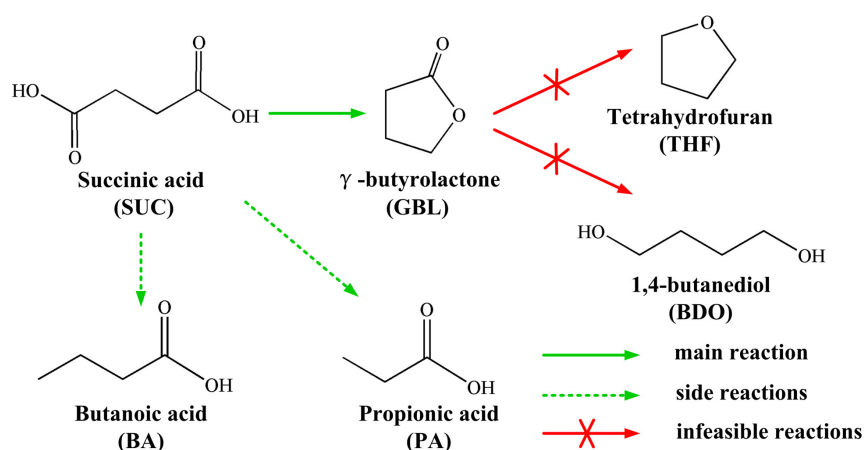
entries	Catalysts	Succinic acid Conversion (mol. %) ^a	γ-butyrolactone Selectivity (mol. %) ^b	Pd Dispersion (%) ^c	Pd Average size (nm) ^c	Turnover Frequencies (h ⁻¹) ^d
1	ZrO ₂	0	0	-	-	-
2	0.1 Pd/ZrO ₂	34	99	65.3	0.8	714
3	0.2 Pd/ZrO ₂	63	95	51.6	1.0	732
4	0.2 Pd/ZrO ₂ ^e	67	94	51.6	1.0	780
5	0.2 Pd/ZrO ₂ ^f	54	95	51.6	1.0	847
6	0.5 Pd/ZrO ₂	85	86	48.8	2.1	468
7	1.0 Pd/ZrO ₂	99 ^g	85 ^g	45.5	2.5	320
8	2.0%Pd/TiO ₂ ^h	90	88	13.0	-	21 ⁱ
9	2.1%Pd/TiO ₂ ^j	94	90	28.0	-	6 ⁱ
10	2.0%Ru/C ^k	72	66	-	-	-

^a reaction conditions: 0.4 g SUC and 0.2 g catalyst in 40.0 mL water at 473 K, 10 MPa and 600 rpm, reaction time is 33 h unless otherwise mentioned; ^b selectivity to GBL; ^c Pd dispersion and average size are determined by H₂ chemisorption and AC-HAADF-STEM; ^d turnover frequencies (TOFs) were calculated based on moles of SUC converted at an initial reaction time of 0.25 h per mole of Pd per hour; ^e 2.0 g SUC in 40.0 mL water; ^f 4.0 g SUC in 40.0 mL water; ^g reaction time is 24 h; ^h reaction conditions: 6.0 g SUC and 1.0 g catalyst in 114.0 g water at 433 K and 15 MPa, reaction time is 48 h [22]; ⁱ TOFs were calculated at the reaction time of 1 h; ^j reaction conditions: 5.0 g SUC and 1.0 g catalyst in 95.0 g water at 433 K and 15 MPa, reaction time is 48 h [24]; ^k reaction conditions: 15.0 g SUC and 1.0 g catalyst in 85.0 g water at 453 K and 15 MPa, reaction time is 35 h [29].

The effects of the SUC concentration on the catalytic performance are listed in Table 1 (entries 3–5). When the SUC concentration is increased from 1.0 wt. % (0.4 g SUC in 40 mL H₂O) to 5.0 wt. % (2.0 g SUC in 40 mL H₂O), the SUC conversion and GBL selectivity over 0.2 Pd/ZrO₂ remain basically constant within the range of experimental error in aqueous solution. The SUC conversion is lower while the selectivity of GBL remains unchanged when the SUC concentration increases to 10.0 wt. % (4.0 g SUC in 40 mL H₂O). The atomically dispersed noble metal particles with small size are generally favored for the formation of a specific product using a different reaction route [5]. Thus, the subnanometer Pd clusters possess similar activity with uniform size and have specific selectivity to GBL (~95%) with the enhanced SUC concentration. Moreover, the SUC over 0.2 Pd/ZrO₂ can be completely converted over a long reaction time of 58 h (Figure S4a). GBL is still the main product and overhydrogenated products (THF and BDO) have yet not been detected.

The supported metal catalysts generally have types of metal particles with broad size distributions and each metal particle may possess multiple active species, which leads to reduced selectivity to the target product [5]. The catalytic performance, depending on the sizes of noble metals, can also be elucidated in Table 1 including comparative literatures [22,24,29]. The selectivity to GBL is reduced from 99% to 85% (entries 2–7) with an average particle size raised from 0.8 nm to 2.5 nm, owing to the increased multiple active species. With the similar conversion of about 54% (Figure S4b), the selectivities to GBL over 0.2 Pd/ZrO₂, 0.5 Pd/ZrO₂ and 1.0 Pd/ZrO₂ are 96%, 87% and 86% (Figure S4c), respectively, which presents a similar trend shown in Table 1 (entries 3–7). The well-defined subnanometer Au clusters as hydrogenation catalysts were previously reported to control the selectivity for α,β-unsaturated alcohols for the C=O bond hydrogenation of α,β-unsaturated

ketones (or aldehyde). The α,β -unsaturated alcohol as the intermediate could not be continuously hydrogenated into saturated alcohol [42]. SUC is mainly transformed into GBL from the first hydrogenation step, and subsequently converted into small quantities of THF and BDO. In our work, the subnanometer Pd clusters are highly specific for the hydrogenation of SUC to GBL and avoid the further hydrogenation of GBL (Scheme 1). On the other hand, the reported Pd catalysts with a size of 2~10 nm can catalyze the subsequent hydrogenation of GBL into BDO and THF [21,22]. Accordingly, the selectivity is extremely sensitive to the metal nanoparticle size [43]. Further, the formation of PA or BA does not originate from the C–C bond breaking of BDO and it occurs via the C–C cracking of succinic acid due to the catalytic activity of hydrogenolysis for the Pd-base catalysts [40,41]. Therefore, the main (formation of GBL) and side reactions (formation of PA and BA) occur independently.



Scheme 1. Reaction routes of succinic acid catalytic hydrogenation over subnanometer Pd clusters.

Moreover, the reported catalysts for the hydrogenation of SUC in water under different reaction conditions (temperature and H₂ pressure) are also listed in Table 1, entries 8–10. As a result, the turnover frequencies (TOFs) for low loadings of Pd/ZrO₂ (0.1 wt. % and 0.2 wt. %) are ~50 times higher than the reported 2.1% Pd/TiO₂ based on the hydrogenation of SUC reaction with higher H₂ pressure (15 MPa) and lower reaction temperature (433 K). For the high-loading Pd samples (0.5 wt. % and 1.0 wt. %), the TOFs are also ~30 times more active than the 2.1% Pd/TiO₂. These results demonstrate the high catalytic performance of the subnanometer Pd cluster catalysts. Similar results have been reported for the small Pd clusters on La-stabilized alumina, which shows higher reactivity in the CO oxidation than the large particles [44]. Moreover, both SUC conversion and the selectivity to GBL on the reported Ru/C are lower than those on the Pd/ZrO₂ catalysts (entry 10). Further, the Ru catalyst can catalyze GBL into THF and BDO with severe carbon loss of as high as 63% in water solvent [29].

In addition, the catalytic activities of the supported metal catalysts could be related to metal-support interactions and the distributions of metal species on support. The mutual effect between the noble metal and the support makes metal clusters behave differently from their nanoparticle counterparts [45,46]. The smaller clusters may create more active sites around the metal-support interface. Conversely, the growth of particles likely loses the metal-support interface that gradually inhibits the ability of the adsorbed species to turn over at the metal-support boundary [47]. Furthermore, very small metal clusters with electronic quantum size effects, in other words the highest occupied molecular orbital-lowest unoccupied molecular orbital (HOMO-LUMO) energy gap, lead to lower activation barriers of the reaction, which have a decisive role in the increase of reactivity [48]. Therefore, the very small metal clusters, especially isolated single atoms, anchored on the supports represent a new type of catalyst with a superior catalytic performance for various reactions [5,8–10]. Thus, the 0.2 Pd/ZrO₂ with an average Pd cluster size of 1.0 nm shows higher catalytic activities for

SUC hydrogenation than those of 0.5 Pd/ZrO₂ and 1.0 Pd/ZrO₂ with Pd cluster sizes of 2.1 nm and 2.5 nm, respectively.

Arrhenius-type plots of the selective hydrogenation of SUC over the Pd/ZrO₂ catalysts are shown in Figure 3 and the activation energy (Ea) was calculated based on initial reaction rates measured at different temperatures. The obtained Ea of $25.0 \pm 1.5 \text{ kJ} \cdot \text{mol}^{-1}$ is similar for all the catalysts. Moreover, when the Pd loading is increased from 0.05 wt. % to 0.2 wt. %, the additional 0.15 wt. % Pd species significantly enhances the reaction rate; however, it does not change the Ea. On the other hand, both the rate and Ea remain constant when the Pd loading is enhanced from 0.2 wt. % to 1.0 wt. %. The results indicate that the presence of additional Pd (0.8 wt. %) in 1.0 Pd/ZrO₂ neither increases the rate nor changes the Ea of the reaction, which is in agreement with previous reports [49]. It is also reported that only the atomically dispersed Au rather than nanoparticles is associated with the active species for the water-gas shift reaction over Au/CeO₂ catalysts and the excess Au neither increases the reaction rate nor changes the Ea [50].

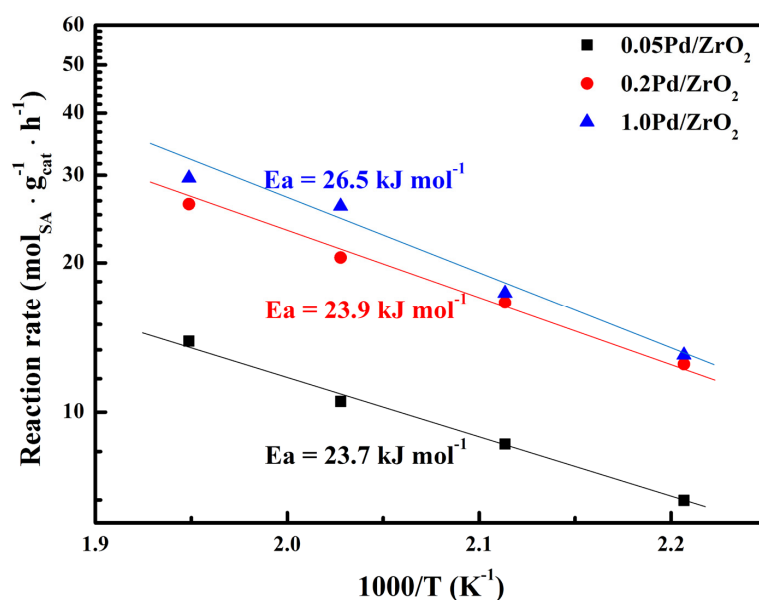


Figure 3. Arrhenius plots of reaction rates over Pd/ZrO₂ catalysts with different Pd loadings.

Figure 4 presents the changes in TOFs over Pd loadings and dispersion during the initial period (Figure S4) of Pd/ZrO₂ catalysts. It is interesting to note a non-linear relationship between TOFs and Pd loadings (or dispersion). The TOFs in Figure 4 are almost unchanged at low Pd loadings (≤ 0.2 wt. %) or high Pd dispersion (>50%), and then decrease with increased Pd loadings [51]. When the size of the Pd particles decreases to the atomic dispersion level, the TOFs remain unchanged. This phenomenon indeed reveals that the catalytic active species are subnanometer Pd clusters. The similar TOFs for the low Au loadings (≤ 0.08 wt. %) have been reported on ZrO₂-supported isolated Au³⁺ ions which are atomically dispersed and isolated from each other for the chemoselective hydrogenation of unsaturated 1,3-butadiene [51]. The TOFs decrease sharply with increased Pd loadings (Figure 4a) and decreased Pd dispersion (Figure 4b) which is associated with the transition of palladium from atomical dispersion to metallic nanoparticles. Similar results have also been reported for the oxidation and hydrogenation reactions using atomically dispersed Au and Pd catalysts [32,52]. Thus, these subnanometer Pd clusters supported on zirconia for SUC hydrogenation with low loadings or high dispersion of Pd and high selectivity to GBL indicate promising applicability.

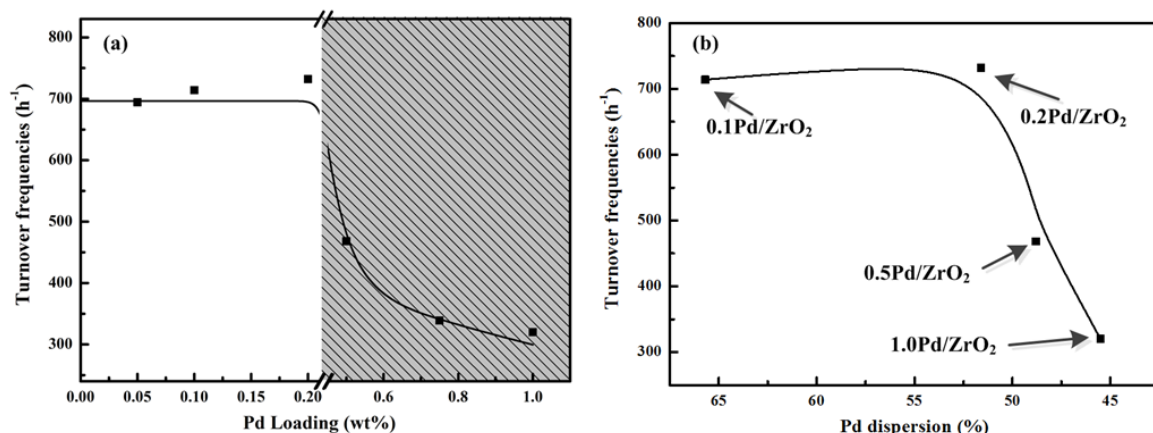


Figure 4. Turnover frequencies as function of Pd Loadings (a) and dispersion (b) for Pd/ZrO₂ catalysts.

2.3. Stability of Pd/ZrO₂ Catalysts

The active metal leaching or sintering of the active species with a loss in catalytic activity during reaction often occurs over the heterogeneous catalysts. Contributions to the stabilization of precious metal catalysts for the hydrogenation of SUC using water as a solvent are very scarce [29]. Therefore, it is necessary to investigate the stability of the supported subnanometer Pd clusters, especially under high temperature, for practical applications.

The thermogravimetric analysis (Figure S5) was conducted to study the thermal stability of the catalyst for the hydrogenation of SUC. The first weight loss of 8% at about 373 K resulted from desorption of physically adsorbed H₂O. The anchored ethoxy groups thermally decomposed on the surface of the sample generates the fast weight loss of 28% between 540 K and 550 K. These species have been observed to be associated with the decomposition of zirconia precipitates prepared in organic medium, where a small quantity of alkyl groups bound to the surface oxygen atoms of the support have been detected [53,54]. Moreover, no weight loss over 550 K indicates the catalysts are fully crystallized under the calcinated temperature of 573 K and should be thermally stable during the reaction process. Moreover, the TGA results of multi-used catalyst (dashed line in Figure S5) further confirm the thermal stability of the 0.2 Pd/ZrO₂ catalyst.

Accordingly, the reusability tests of this catalyst are shown in Figure 5. A slight fluctuation of SUC conversion (~65%) and GBL selectivity (~95%) was observed. In addition, inductively coupled plasma atomic emission spectroscopy characterization on the fresh catalysts and the used catalyst after 33 h hydrogenation was performed to determine the Pd leaching during the reaction process (Table S1). The similar loading between the fresh (0.22 wt. %) and used (0.21 wt. %) 0.2 Pd/ZrO₂ catalysts indicate no leaching of Pd species. Moreover, SA conversion remains unchanged in a hot-filtered solution without solid catalyst after 10 h under the same reaction conditions. These results mean no leaching of Pd species and are consistent with recycling experiments. Besides, no collapse of the pores in the support occurs under the reaction conditions that can be determined from the BET surface area of 0.2 Pd/ZrO₂ before and after the catalytic reaction (Table S1). Further, the XRD pattern of the sixth recycled catalyst (Figure S3) shows the same peaks as the fresh catalysts, which confirms the stability of the catalyst. Therefore, the stable and reusable Pd/ZrO₂ catalysts could serve as promising catalysts in the hydrogenation of SUC in water.

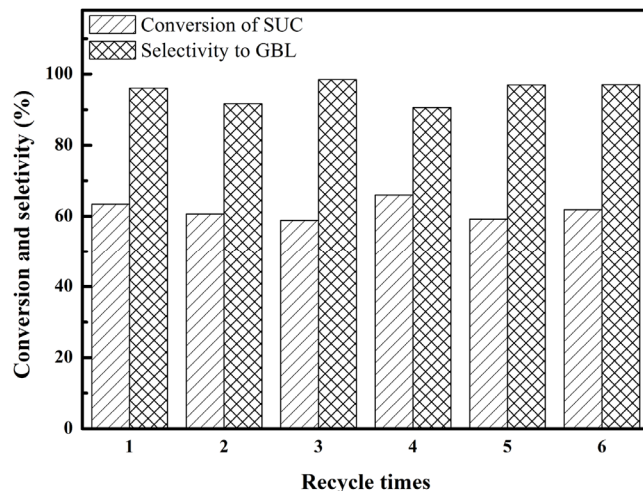


Figure 5. Recycling experimental results of 0.2 Pd/ZrO₂ catalyst.

3. Materials and Methods

Atomically dispersed Pd supported on zirconia were prepared by a microwave-assisted hydrothermal method using K₂PdCl₄ (>99.9%, Aladdin Chemistry Co. Ltd., Shanghai, China) as palladium source and zirconium oxynitrate hydrate (>99.5%, Aladdin Chemistry Co. Ltd., Shanghai, China) as zirconium source. Prior to microwave hydrothermal irradiation, the zirconium oxynitrate hydrate was dissolved in ethanol and K₂PdCl₄ solution was added to the mixture based on the Pd loading. After stirring for 30 min, the homogeneous mixture was transferred into a high-pressure vessel with a magnetic stirrer. Next, the vessel was placed in a microwave reactor (Mars 450, CEM Corp., Matthews, NC, USA), which was set at 2.45 GHz with a power of 400 W and maintained at 393 K for 120 min with stirring. Finally, the products were dried at 333 K for 12 h followed by calcination at 573 K for 3 h. The catalysts prepared were identified as m Pd/ZrO₂, where m represents the weight percentage of Pd based on the total catalyst. Prior to activity tests and characterization, all catalysts were reduced in a tube furnace in 10% H₂/He atmosphere at 573 K for 3 h and stored under vacuum in the dark.

Aberration-corrected high-angle annular dark-field images were obtained on a ChemiSTEM using a scanning transmission electron microscopy (Titan G² 80-200, FEI Corp., Hillsboro, CA, USA) at 200 kV with probe size of ~1.3 Å. The energy-dispersive X-ray analysis element mappings were also conducted under HAADF mode from the same microscope. The HAADF images were formed through collecting transmitted electrons with an annular detector from an angle of 22 mrad.

X-ray diffraction characterization was performed on the X'Pert PRO diffractometer (PW3040/60, PANalytical Corp., Egham, England) using a CuK α radiation source ($\lambda = 1.54056 \text{ \AA}$). XRD patterns were recorded in the 2θ range from 10° to 80° with scanning speed of $10^\circ \cdot \text{min}^{-1}$ in continuous mode. Inductively coupled plasma atomic emission spectroscopy were employed to determine the Pd loadings in the catalysts on an XSP instrument (IRIS intrepid II, Thermo Electron Corp., Beverly, MA, USA).

The dispersion of Pd exposed on ZrO₂ surface and average Pd particle sizes for Pd/ZrO₂ catalysts were determined by H₂ chemisorption on a chemisorption analyzer (Autochem 2920, Micromeritics Instrument Corp., Norcross, GA, USA). The dried sample (about 0.1 g) was firstly reduced in a stream of 10% H₂/Ar with $30 \text{ cm}^3 \cdot \text{min}^{-1}$ for 2 h at 753 K and purged with Ar for 1 h at 753 K to remove the absorbed H₂. Then, the catalyst was cooled to 318 K and H₂ pulses were injected through a on-line valve to record the absorption isotherm. Then, the sample was evacuated and the weak adsorption isotherm was ascertained with a second adsorption isotherm.

Adsorption and desorption isotherms of N₂ were measured at 77 K using physisorption analyzer (ASAP 2020, Micromeritics Instrument Corp., Norcross, GA, USA). Before measurement, the samples

were degassed in vacuum for 6 h under the temperature of 573 K. The surface area were determined from the Brunauer-Emmett-Teller equation, respectively. The thermogravimetric analyzer was adopted to analyze the thermal stability of the Pd/ZrO₂ catalysts by a TA instrument (TA Q600, TA Instruments Corp., New Castle, Germany) and was carried out under ambient conditions at a constant flow rate of 100 cm³·min⁻¹ and heating rate (10 K·min⁻¹) with the temperature range of 293–1073 K.

The selective hydrogenation of SUC to GBL was performed in a batch reactor (100 mL, Mini-4560, Parr Corp., Moline, IL, USA) at 473 K and 10 MPa (H₂). Succinic acid (0.4 g to 4.0 g), reduced catalyst (0.2 g) and de-ionized water (40.0 g) as solvent were charged into the reactor. Before heating, H₂ was purged into the reactor four times to remove air in the reactor, and then filled with 6 MPa hydrogen. After heating the reactor to reaction temperature (473 K), hydrogen pressure was raised up to 10 MPa. During the reaction, the reactant was stirred at a speed of 600 rpm to avoid mass transfer limitation. Samples were taken from system every 1–2 h. Reaction products were analyzed using gas (7890A, Agilent, Santa Clara, CA, USA) and liquid (LC-2010A, Shimadzu, Chiyoda-ku, Japan) chromatography. The gas chromatograph uses a SE-54 column and a FID detector to identify GBL, THF and BDO. As for the liquid chromatography, an Inertsil ODS-SP column (5 µm 4.6 mm × 150 mm) was used to separate and identify SUC, GBL, PA and BA.

4. Conclusions

We synthesized highly dispersed subnanometer Pd clusters supported on zirconia using a microwave-assisted hydrothermal method. Through two-dimensional Gaussian function fits of AC-HAADF images, we confirm that Pd species represent small clusters with a size less than 1 nm on the zirconia surface, containing a few of the Pd atoms. The high selectivity for the hydrogenation of SUC to GBL is attributed to the subnanometer Pd clusters, which is also illustrated by the unchanged activation energies and TOFs at low loadings. Further, the atomically dispersed Pd catalyst can be recycled at least six times without an obvious decline in catalytic activity. Thus, this atomically dispersed catalyst with reusability can reduce the consumption of noble metals and provide potential for succinic acid conversion.

Supplementary Materials: The following are available online at www.mdpi.com/2073-4344/6/7/100/s1. Figure S1: AC-HAADF-STEM images of 0.2 Pd/ZrO₂ catalyst, Figure S2: Nitrogen adsorption and desorption isotherms of 0.2 Pd/ZrO₂, Figure S3: XRD patterns of Pd/ZrO₂ before and after reaction, Figure S4: Catalytic activities of SUC hydrogenation over 0.2 Pd/ZrO₂ catalysts (a) and different Pd loadings (b,c), Figure S5: TGA patterns of 0.2 Pd/ZrO₂ and used 0.2 Pd/ZrO₂ catalysts, Table S1: Physicochemical properties of Pd/ZrO₂ catalysts.

Acknowledgments: We gratefully acknowledge the support of the National Natural Science Foundation of China (NSFC 21476084, 21406063, 21576081), the Fundamental Research Funds for the Central Universities, PetroChina Innovation Foundation and the Open Project of Shanghai Key Laboratory of Molecular Catalysis and Innovative Materials (2014MCIMKF02).

Author Contributions: Chi Zhang and Lifang Chen conceived and designed the experiments; Chi Zhang and Wenrong Cao performed the experiments; Chi Zhang and Hongye Cheng analyzed the data; Zhiwen Qi contributed reagents/materials/analysis tools; Chi Zhang wrote the paper.

Conflicts of Interest: The authors declare no conflict of interest.

References

- Izarova, N.V.; Pope, M.T.; Kortz, U. Noble metals in polyoxometalates. *Angew. Chem. Int. Ed.* **2012**, *51*, 9492–9510. [[CrossRef](#)] [[PubMed](#)]
- Gholami, R.; Alyani, M.; Smith, K.J. Deactivation of Pd catalysts by water during low temperature methane oxidation relevant to natural gas vehicle converters. *Catalysts* **2015**, *5*, 561–594. [[CrossRef](#)]
- Manabe, K.; Yamaguchi, M. Catalyst-controlled site-selectivity switching in Pd-catalyzed cross-coupling of dihaloarenes. *Catalysts* **2014**, *4*, 307–320. [[CrossRef](#)]
- Hutchings, G.S.; Zhang, Y.; Li, J.; Yonemoto, B.T.; Zhou, X.G.; Zhu, K.K.; Jiao, F. In situ formation of cobalt oxide nanocubanes as efficient oxygen. *J. Am. Chem. Soc.* **2015**, *137*, 4223–4229. [[CrossRef](#)] [[PubMed](#)]

5. Kwak, J.H.; Kovarik, L.; Szanyi, J. CO₂ reduction on supported Ru/Al₂O₃ catalysts: Cluster size dependence of product selectivity. *ACS Catal.* **2013**, *3*, 2449–2455. [[CrossRef](#)]
6. Lu, H.; Li, W.C.; Hou, Z.; Schuth, S.F. Molecular level dispersed Pd clusters in the carbon walls of ordered mesoporous carbon as a highly selective alcohol oxidation catalyst. *Chem. Commun.* **2007**, 1038–1040. [[CrossRef](#)] [[PubMed](#)]
7. Uzun, A.; Ortalan, V.; Browning, N.D.; Gates, B.C. A site-isolated mononuclear iridium complex catalyst supported on MgO: Characterization by spectroscopy and aberration-corrected scanning transmission electron microscopy. *J. Catal.* **2010**, *269*, 318–328. [[CrossRef](#)]
8. Yan, H.; Cheng, H.; Yi, H.; Lin, Y.; Yao, T.; Wang, C.; Li, J.; Wei, S.; Lu, J. Single-atom Pd₁/graphene catalyst achieved by atomic layer deposition: Remarkable performance in selective hydrogenation of 1, 3-butadiene. *J. Am. Chem. Soc.* **2015**, *137*, 10484–10487. [[CrossRef](#)] [[PubMed](#)]
9. Peterson, E.J.; Delariva, A.T.; Lin, S.; Johnson, R.S.; Guo, H.; Miller, J.T.; Kwak, J.H.; Peden, C.H.F.; Kiefer, B.; Allard, L.F.; et al. Low-temperature carbon monoxide oxidation catalysed by regenerable atomically dispersed palladium on alumina. *Nat. Commun.* **2014**. [[CrossRef](#)] [[PubMed](#)]
10. Hatanaka, M.; Takahashi, N.; Tanabe, T.; Nagai, Y.; Dohmae, K. Ideal Pt loading for a Pt/CeO₂-based catalyst stabilized by a Pt–O–Ce bond. *Appl. Catal. B Environ.* **2010**, *99*, 336–342. [[CrossRef](#)]
11. Chen, L.F.; Hu, J.C.; Richards, R. Intercalation of aggregation-free and well-dispersed gold nanoparticles into the walls of mesoporous silica as a robust “green” catalyst for *n*-alkane oxidation. *J. Am. Chem. Soc.* **2009**, *131*, 914–915. [[CrossRef](#)] [[PubMed](#)]
12. Jirkovsky, J.S.; Panas, I.; Ahlberg, E.; Halasa, M.; Romani, S.; Schiffrin, D.J. Single atom hot-spots at Au–Pd nanoalloys for electrocatalytic H₂O₂ Production. *J. Am. Chem. Soc.* **2011**, *133*, 19432–19441. [[CrossRef](#)] [[PubMed](#)]
13. Yang, M.; Allard, L.F.; Flytzani-Stephanopoulos, M. Atomically dispersed Au–(OH)_x species bound on titania catalyze the low-temperature water-gas shift reaction. *J. Am. Chem. Soc.* **2013**, *135*, 3768–3771. [[CrossRef](#)] [[PubMed](#)]
14. Song, H.; Lee, S.Y. Production of succinic acid by bacterial fermentation. *Enzyme Microb. Techol.* **2006**, *39*, 352–361. [[CrossRef](#)]
15. Binder, J.B.; Raines, R.T. Simple chemical transformation of lignocellulosic biomass into furans for fuels and chemicals. *J. Am. Chem. Soc.* **2009**, *131*, 1979–1985. [[CrossRef](#)] [[PubMed](#)]
16. Corma, A.; Iborra, S.; Velty, A. Chemical routes for the transformation of biomass into chemicals. *Chem. Rev.* **2007**, *107*, 2411–2502. [[CrossRef](#)] [[PubMed](#)]
17. Huang, J.; Dai, W.L.; Fan, K. Remarkable support crystal phase effect in Au/FeO_x catalyzed oxidation of 1, 4-butanediol to γ -butyrolactone. *J. Catal.* **2009**, *266*, 228–235. [[CrossRef](#)]
18. Delhomme, C.; Weuster-Botz, D.; Kühn, F.E. Succinic acid from renewable resources as a C4 building-block chemical—a review of the catalytic possibilities in aqueous media. *Green Chem.* **2009**, *11*, 13–26. [[CrossRef](#)]
19. Gallezot, P. Conversion of biomass to selected chemical products. *Chem. Soc. Rev.* **2012**, *41*, 1538–1558. [[CrossRef](#)] [[PubMed](#)]
20. Hong, U.G.; Hwang, S.; Seo, J.G.; Yi, J.; Song, I.K. Hydrogenation of succinic acid to γ -butyrolactone over palladium catalyst supported on mesoporous alumina xerogel. *Catal. Lett.* **2010**, *138*, 28–33. [[CrossRef](#)]
21. Chung, S.H.; Park, Y.M.; Kim, M.S.; Lee, K.Y. The effect of textural properties on the hydrogenation of succinic acid using palladium incorporated mesoporous supports. *Catal. Today* **2012**, *185*, 205–210. [[CrossRef](#)]
22. Tapin, B.; Epron, F.; Espezel, C.; Ly, B.K.; Pinel, C.; Besson, M. Study of monometallic Pd/TiO₂ catalysts for the hydrogenation of succinic acid in aqueous phase. *ACS Catal.* **2013**, *3*, 2327–2335. [[CrossRef](#)]
23. Hong, U.G.; Park, H.W.; Lee, J.; Hwang, S.; Yi, J.; Song, I.K. Hydrogenation of succinic acid to tetrahydrofuran (THF) over rhenium catalyst supported on H₂SO₄-treated mesoporous carbon. *Appl. Catal. A Gen.* **2012**, *415*, 141–148. [[CrossRef](#)]
24. Ly, B.K.; Minh, D.P.; Pinel, C.; Besson, M.; Tapin, B.; Epron, F.; Espezel, C. Effect of addition mode of Re in bimetallic Pd-Re/TiO₂ catalysts upon the selective aqueous-phase hydrogenation of succinic acid to 1, 4-Butanediol. *Top Catal.* **2012**, *55*, 466–473. [[CrossRef](#)]
25. Hara, Y.; Kusaka, H.; Inagaki, H.; Takahashi, K.; Wada, K. A novel production of γ -butyrolactone catalyzed by ruthenium complexes. *J. Catal.* **2000**, *194*, 188–197. [[CrossRef](#)]
26. Deshpande, R.M.; Buwa, V.V.; Rode, C.V.; Chaudhari, R.V.; Mills, P.L. Tailoring of activity and selectivity using bimetallic catalyst in hydrogenation of succinic acid. *Catal. Commun.* **2002**, *3*, 269–274. [[CrossRef](#)]

27. Luque, R.; Lin, C.S.K.; Du, C.; Macquarrie, D.J.; Koutinas, A.; Wang, R.; Webb, C.; Clark, J.H. Chemical transformations of succinic acid recovered from fermentation broths by a novel direct vacuum distillation-crystallisation method. *Green Chem.* **2009**, *11*, 193–200. [[CrossRef](#)]
28. Minh, P.; Besson, M.; Pinel, C.; Fuertes, P.; Petitjean, C. Aqueous-phase hydrogenation of biomass-based succinic acid to 1,4-butanediol over supported bimetallic catalysts. *Top. Catal.* **2010**, *53*, 1270–1273. [[CrossRef](#)]
29. Di, X.; Shao, Z.; Li, C.; Li, W.; Liang, C. Hydrogenation of succinic acid over supported rhenium catalysts prepared by the microwave-assisted thermolytic method. *Catal. Sci. Technol.* **2015**, *5*, 2441–2448. [[CrossRef](#)]
30. Ly, B.K.; Tapin, B.; Aouine, M.; Delichere, P.; Epron, F.; Pinel, C.; Espezel, C.; Besson, M. Insights into the oxidation state and location of rhenium in Re-Pd/TiO₂ catalysts for aqueous-phase selective hydrogenation of succinic acid to 1,4-butanediol as a function of palladium and rhenium deposition methods. *ChemCatChem* **2015**, *7*, 2161–2178. [[CrossRef](#)]
31. Qiao, B.; Wang, A.; Yang, X.; Allard, L.; Jiang, Z.; Cui, Y.; Liu, J.; Li, J.; Zhang, T. Single-atom catalysis of CO oxidation using Pt₁/FeO_x. *Nat. Chem.* **2011**, *3*, 634–641. [[CrossRef](#)] [[PubMed](#)]
32. Hackett, S.F.J.; Brydson, R.M.; Gass, M.H.; Harvey, I.; Newman, A.D.; Wilson, K.; Lee, A.F. High-activity, single-site mesoporous Pd/Al₂O₃ catalysts for selective aerobic oxidation of allylic alcohols. *Angew. Chem. Int. Ed.* **2007**, *46*, 8593–8596. [[CrossRef](#)] [[PubMed](#)]
33. Zhang, C.; Chen, L.F.; Cheng, H.Y.; Zhu, X.D.; Qi, Z.W. Atomically dispersed Pd catalysts for the selective hydrogenation of succinic acid to γ -butyrolactone. *Catal. Today* **2016**. [[CrossRef](#)]
34. Jentys, A. Estimation of mean size and shape of small metal particles by EXAFS. *Phys. Chem. Chem. Phys.* **1999**, *1*, 4059–4063. [[CrossRef](#)]
35. Efremenko, I.; German, E.D.; Sheintuch, M. Density functional study of the interactions between dihydrogen and Pd_n ($n = 1$ –4) clusters. *J. Phys. Chem. A* **2000**, *104*, 8089–8096. [[CrossRef](#)]
36. Zhu, P.; Zhang, J.; Wu, Z.; Zhang, Z. Microwave-assisted synthesis of various ZnO hierarchical nanostructures: Effects of heating parameters of microwave oven. *Cryst. Growth Des.* **2008**, *8*, 3148–3153. [[CrossRef](#)]
37. Yang, G.; Kong, Y.; Hou, W.; Yan, Q. Heating behavior and crystal growth mechanism in microwave field. *J. Phys. Chem. B* **2005**, *109*, 1371–1379. [[CrossRef](#)] [[PubMed](#)]
38. Ugalde, M.; Chavira, E.; Figueroa, I.A.; Quintanar, C.; Espinosa-Magana, F.; Zaragoza-Contreras, E.A.; Ochoa-Lara, M.T. Preparation of rhodium nano-particles using microwaves. *J. Sol Gel Sci. Technol.* **2013**, *65*, 311–317. [[CrossRef](#)]
39. You, C.J.; Zhang, C.; Chen, L.F.; Zhu, X.D.; Qi, Z.W. Highly dispersed palladium nanoclusters incorporated in amino-functionalized silica spheres for the selective hydrogenation of succinic acid to γ -butyrolactone. *Appl. Organomet. Chem.* **2015**, *29*, 653–660. [[CrossRef](#)]
40. Hong, U.G.; Lee, J.; Hwang, S.; Song, I.K. Hydrogenation of succinic acid to γ -butyrolactone (GBL) over palladium-alumina composite catalyst prepared by a single-step sol-gel method. *Catal. Lett.* **2011**, *141*, 332–338. [[CrossRef](#)]
41. Hong, U.G.; Hwang, S.; Seo, J.G.; Lee, J.; Song, I.K. Hydrogenation of succinic acid to γ -butyrolactone (GBL) over palladium catalyst supported on alumina xerogel: Effect of acid density of the catalyst. *J. Ind. Eng. Chem.* **2011**, *17*, 316–320. [[CrossRef](#)]
42. Liu, Y.M.; Tsunoyama, H.; Akita, T.; Xie, S.; Tsukuda, T. Aerobic oxidation of cyclohexane catalyzed by size-controlled Au clusters on hydroxyapatite: Size effect in the sub-2 nm regime. *ACS Catal.* **2011**, *1*, 2–6. [[CrossRef](#)]
43. Lei, Y.; Mehmood, F.; Lee, S.; Greeley, J.; Lee, B.; Seifert, S.; Winans, R.E.; Elam, J.W.; Meyer, R.J.; Redfern, P.C.; et al. Increased silver activity for direct propylene epoxidation via subnanometer size effects. *Science* **2010**, *328*, 224–228. [[CrossRef](#)] [[PubMed](#)]
44. Gaudet, J.R.; Riva, A.; Peterson, E.J.; Bolin, T.; Datye, A.K. Improved low-temperature CO oxidation performance of Pd supported on La-stabilized alumina. *ACS Catal.* **2013**, *3*, 846–855. [[CrossRef](#)]
45. Favera, N.D.; Kiehne, U.; Bunzen, J.; Hytteballe, S.; Lützen, A.; Piguet, C. Intermetallic interactions within solvated polynuclear complexes: A misunderstood concept. *Angew. Chem. Int. Ed.* **2010**, *49*, 125–128. [[CrossRef](#)] [[PubMed](#)]
46. Pulido, A.; Oliver-Tomas, B.; Renz, M.; Boronat, M.; Corma, A. Ketonic decarboxylation reaction mechanism: A combined experimental and DFT study. *ChemSusChem* **2013**, *6*, 141–151. [[CrossRef](#)] [[PubMed](#)]

47. Zhang, S.; Chang, C.R.; Huang, Z.Q.; Li, J.; Wu, Z.; Ma, Y.; Qu, Y. High catalytic activity and chemoselectivity of sub-nanometric Pd clusters on porous-nanorods of CeO₂ for hydrogenation of nitroarenes. *J. Am. Chem. Soc.* **2016**, *138*, 2629–2637. [CrossRef] [PubMed]
48. Souza, P.M.; Rabelo-Neto, R.C.; Borges, L.E.; Jacobs, G.; Davis, B.H.; Graham, U.M.; Noronha, F.B. Effect of zirconia morphology on hydrodeoxygenation of phenol over Pd/ZrO₂. *ACS Catal.* **2015**, *5*, 7385–7398. [CrossRef]
49. Lopez-Acevedo, O.; Kacprzak, K.A.; Akola, J.; Häkkinen, H. Quantum size effects in ambient CO oxidation catalysed by ligand-protected gold clusters. *Nat. Chem.* **2010**, *2*, 329–334. [CrossRef] [PubMed]
50. Fu, Q.; Saltsburg, H.; Flytzani-Stephanopoulos, M. Active nonmetallic Au and Pt species on ceria-based water-gas shift catalysts. *Science* **2003**, *301*, 935–938. [CrossRef] [PubMed]
51. Zhang, X.; Shi, H.; Xu, B.Q. Catalysis by gold: Isolated surface Au³⁺ ions are active sites for selective hydrogenation of 1,3-butadiene over Au/ZrO₂ catalysts. *Angew. Chem. Int. Ed.* **2005**, *44*, 7132–7135. [CrossRef] [PubMed]
52. Guan, Y.; Hensen, E.J.M. Cyanide leaching of Au/CeO₂: Highly active gold clusters for 1,3-butadiene hydrogenation. *Phys. Chem. Chem. Phys.* **2009**, *11*, 9578–9582. [CrossRef] [PubMed]
53. Figueroa, S.; Desimoni, J.; Rivas, P.C.; Cervera, M.M.; Caracoche, M.C. Hyperfine study on sol-gel derived-hematite doped zirconia. *Chem. Mater.* **2005**, *17*, 3486–3491. [CrossRef]
54. Chen, L.F.; Hu, J.C.; Richards, R.M. Catalytic properties of nanoscale iron-doped zirconia solid-solution aerogels. *ChemPhysChem* **2008**, *9*, 1069–1078. [CrossRef] [PubMed]



© 2016 by the authors; licensee MDPI, Basel, Switzerland. This article is an open access article distributed under the terms and conditions of the Creative Commons Attribution (CC-BY) license (<http://creativecommons.org/licenses/by/4.0/>).